ISSN 1023-1935, Russian Journal of Electrochemistry, 2015, Vol. 51, No. 5, pp. 458–467. © Pleiades Publishing, Ltd., 2015.
Original Russian Text © V.A. Sadykov, E.M. Sadovskaya, N.F. Uvarov, 2015, published in Elektrokhimiya, 2015, Vol. 51, No. 5, pp. 529–539.

Methods of Isotopic Relaxations for Estimation of Oxygen Diffusion Coefficients in Solid Electrolytes and Materials with Mixed Ionic-Electronic Conductivity

V. A. Sadykov[a, b, z], E. M. Sadovskaya[a, b], and N. F. Uvarov[c]

[a] *Boreskov Institute of Catalysis, Siberian Branch, Russian Academy of Sciences, pr. akad. Lavrent'eva 5, Novosibirsk, 630090 Russia*

[b] *Novosibirsk State University, ul. Pirogova 2, Novosibirsk, 630090 Russia*

[c] *Institute of Solid State Chemistry and Mechanochemistry, Siberian Branch, Russian Academy of Sciences, Novosibirsk, Russia*

Received July 31, 2014

Abstract—Theoretical basis of isotopic oxygen exchange in a gas–solid oxide system are considered. A generalized model is suggested that accounts for diffusion of tracer oxygen atoms and allows within a single approach to perform numeric analysis of isotope experiments implemented in reactors of various types and in different temperature modes. It is shown that when $C^{18}O_2$ is used as an isotopic reagent, the oxygen exchange rate on the metal oxide surface increases manifold (as compared to $^{18}O_2$), which allows determining more precisely diffusion limitations in case of isotopic exchange of oxygen in the oxide bulk. Estimates of oxygen self-diffusion coefficients are obtained in dispersed systems based on doped cerium–zirconium oxides with a fluorite-type structure, doped lanthanum silicates with an apatite-type structure, and also mixed praseodymium nickelates–cobaltites and their composites with yttrium–doped ceria.

Keywords: isotopic exchange of oxygen, self-diffusion, doped cerium–zirconium oxides, doped lanthanum silicates, mixed praseodymium nickelates–cobaltites, composites

DOI: 10.1134/S1023193515050109

INTRODUCTION

Development of high–performance intermediate–temperature fuel cells with nanocomposite cathodes and anodes, oxygen-conducting membranes, nanocomposite catalysts of biofuel transformation into syngas requires reliable estimation of oxygen mobility in dispersed materials/porous layers. Here, the most effective method is the SSITKA method of isotopic relaxations (Steady-State Isotopic Transient Kinetic Analysis) [1–3]. As opposed to the known methods of analysis of relaxations of conductivity, mass, and spatial profiles of oxygen isotopes in compact ceramics, analysis of relaxation of isotopic composition of the gaseous reagent in case of isotopic exchange with dispersed oxide oxygen allows determining not only average–integral diffusion coefficients of oxygen [4–6], but also detecting oxygen forms with different mobility in the solid oxide bulk [7–9]. This communication considers theoretical fundamentals of the dynamics of oxygen isotopic exchange in the gas–solid oxide system, techniques of conducting isotopic experiments and methods of analysis of isotopic–kinetic data obtained in isothermic and temperature–programmed experiments in both flow–through and static setups. The results of systematic studies of the oxygen diffusion rate in dispersed materials with ionic and mixed ionic-electronic conductivity with fluorite, apatite, and perovskite structure are presented.

Systems with a fluorite-type structure based on doped cerium–zirconium mixed oxides can be used both as anodes of solid oxide fuel cells and as catalysts. Mobility of lattice oxygen is an important factor determining high performance and stable operation of such systems. Introduction of rare–earth metal cations into cerium–zirconium mixed oxides stabilizes their structure and allows regulating oxygen mobility [10, 11].

Of great interest in the recent years are lanthanum silicates with the apatite structure as a promising class of solid electrolytes for intermediate–temperature solid oxide fuel cells [12–15]. Doped lanthanum silicates are stable both under oxidizing and reducing conditions and feature high ionic conductivity comparable with that of gadolinium–doped ceria at lower conductivity activation energy. This is due to specifics of ionic transport in such systems provided, as opposed to conventional solid electrolytes with perovskite and fluorite structures, by the presence of interstitial oxygen ions. In general, the apatite structure can be represented by the crystallographic formula of $M_{10}(RO_4)_6X_2$, where M $=La^{3+}$, Mg^{2+}, Ca^{2+} etc.;

[z] Corresponding author: vasadykov@mail.ru (V.A. Sadykov).

Table 1. Values of oxygen self-diffusion coefficients at $t = 500°C$ and diffusion activation energies on samples of lanthanum silicates with an apatite structure

Sample	t^*_{ann}, °C	S^{**}, m^2/g	D, cm^2/s (exchange with $C^{18}O_2$)	E_D, kJ/mol (exchange with $C^{18}O_2$)	D, cm^2/s (SIMS)
$La_{9.83}Si_5Al_{0.75}Fe_{0.25}O_{26.5}$	900	5	0.2×10^{-10}	70	
$La_{9.83}Si_5Al_{0.75}Fe_{0.25}O_{26.5}$	1200	1.2	0.8×10^{-10}	90	
$La_{10}Si_{5.5}Fe_{0.5}O_{26.5}$	1200	2	2×10^{-10}	90	
$La_{9.83}Si_{4.5}Fe_{1.5}O_{26}$ [26]	1400	Compact pellet			1×10^{-10}

* t_{ann} is the sample annealing temperature.
** S is the specific surface area of the samples.

$R = Si^{4+}$, Ge^{4+}, P^{5+} etc.; $X = O^{2-}$, OH^-, F^- etc. It can be described as consisting of isolated tetrahedral RO_4 anions and M cations located in 9-coordinated 4*f* sites or 7-coordinated 6*h* positions [13]. Seven–coordinated cations form channels along the *c* axis that contain X anions. It is assumed that it is these oxygen anions that provide high ionic conductivity of rare–earth silicates with an apatite structure. However, only defect systems with cation vacancies ($La_{9.33}Si_6O_{26}$) or excess of oxygen ($La_{9.67}Si_6O_{26.5}$, $La_9SrSi_6O_{26.5}$) feature high conductivity, while stoichiometric systems ($La_8Sr_2Si_6O_{26}$) are characterized by low conductivity. This was explained by a shift of anions in the channels of nonstoichiometric apatites from the center to interstitial sites with formation of additional interstitial anions due to condensation of silicate groups etc [15]. Partial replacement of silicon by aluminum or iron also results in an increase in conductivity, which was primarily explained by an increase in the lattice cell size and therefore the size of transport channels [16].

Cathodic materials based on perovskites doped by alkali–earth cations (LS(F)C, BSCF etc.) used at present provide high power density in solid oxide fuel cells with thin layers of electrolyte (YSZ, ScCeSZ) supported on planar NiO–YSZ anodes protected by buffer layers of gadolinium– or yttrium–doped ceria (GDC, YDC). However, such doped perovskites interact in the intermediate–temperature range with CO_2 and water present in air, which leads to segregation of Ba/Sr hydroxides and carbonates/hydroxocarbonates in the surface layer. The related blocking of active surface centers corresponding to transition metal cations is reflected in degradation of the operating characteristics of cathodes. Obviously, the possible solution of this problem consists in development of cathodic materials with high oxygen mobility and reactivity free of alkali–earth cations. Of greatest interest among the promising systems of this type are lanthanoid nickelates Ln_2NiO_4 with a Ruddlesden–Popper structure, mixed lanthanoid nickelates–cobaltites $LnNi_{1-x}Co_xO_3$ (Ln = La, Pr) and their composites with doped ceria that indeed demonstrate power density values of solid oxide fuel cells (SOFC) promising for practical application [17–20].

Thus, the choice for studies of oxygen diffusion characteristics in these systems is determined both by their practical significance and great attention paid in modern studies to establishment of fundamental factors determining oxygen mobility in the systems with fast ionic conductivity.

EXPERIMENTAL

Synthesis of Samples

Doped cerium–zirconium mixed oxide with fluorite structure with supported platinum. Dispersed oxide $Pr_{0.3}Ce_{0.35}Zr_{0.35}O_2$ was synthesized using the method of polymerized ester precursors (Pecchini) and was sintered in air at 700°C. Platinum (1.4 wt %) was supported using incipient wetness impregnation with H_2PtCl_6 solution followed by drying and annealing in air at 500°C for 2 h. The results of detail studies of the real structure and surface characteristics of such systems using a combination of diffraction (XRD, neutron diffraction, high–resolution electron microscopy), spectroscopic (fine structure of absorption spectra of X-ray synchrotron radiation, secondary ion mass spectrometry (SIMS), X-ray photoelectron spectroscopy (XPS), IR spectroscopy of adsorbed CO test molecules), and magnetic methods are presented in a number of papers [21, 22].

Doped lanthanum silicates with an apatite structure (LSA). Samples were prepared using the method of mechanochemical activation of a mixture of $La(OH)_3$ and amorphous $SiO_2 \cdot nH_2O$ impregnated by aqueous $Fe(NO_3)_3$ or $Al(NO_3)_3$ solutions with the further drying at 50°C. A stoichiometric mixture of the initial compounds (10–30 g) was activated for 20–35 min in an AGO-2 planetary mill with steel drums cooled by water. The activation products were annealed at different temperatures of 900–1200°C for 3–8 h [15, 16]. The composition and specific surface areas of the studied samples are presented in Table 1.

Table 2. Values of diffusion coefficients (at 500°C) and activation energies characterizing different oxygen forms in praseodymium nickelate–cobaltite samples and their composites. The percentage of oxygen corresponding to the given diffusion coefficient is presented in brackets

Sample	S^*, m^2/g	$D_1 \times 10^9$, cm^2/s	E_{D_1}, kJ/mol	$D_2 \times 10^{12}$, cm^2/s	E_{D_2}, kJ/mol
$PrNi_{0.6}Co_{0.4}$	2	0.1 (5–10%)	120	1.3 (>90%)	180
$PrNi_{0.6}Co_{0.4}O_3 + Ce_{0.9}Y_{0.1}O_2$	2	2.0 (60%)	130	0.1 (40%)	
$PrNi_{0.5}Co_{0.5}$	1.7	0.5 (5–10%)	120	2 (>90%)	
$PrNi_{0.5}Co_{0.5}O_3 + CeYO_2$	1.7	3.0 (60%)	130	0.6 (40%)	
$PrNi_{0.4}Co_{0.6}$	1.5	0.1 (5–10%)	120	0.8 (>90%)	
$PrNi_{0.4}Co_{0.6}O_3 + CeYO_2$	1.5	1.0 (60%)	120	0.1 (40%)	

S is the specific surface area of the samples.

Mixed praseodymium nickelates–cobaltites with perovskite structure and their composites. Complex oxides $PrNi_{1-x}Co_xO_{3+\delta}$ ($x = 0$–0.6) and $Ce_{0.9}Y_{0.1}O_{2-\delta}$ (YDC) were synthesized using the modified Pecchini method [20, 21]. Composites were manufactured using the ultrasonic dispersion technique (a T25 ULTRA-TURRAX IKA disperser, Germany) of a mixture of dispersed praseodymium nickelates–cobaltites annealed at 700°C and YDC (at the weight ratio of 1 : 1) in isopropanol with addition of 1 wt % polyvinylbutyral with the further drying at the room temperature. Perovskites and nanocomposites were compacted into pellets, dried in air at 1000°C, and then ground to powders. The composition and specific surface areas of the studied samples are presented in Table 2.

Isotopic Exchange

Isotopic exchange in a closed reactor. The setup for isotopic exchange in the static mode consists of an storage volume and a quartz reactor (with the volume of 145 cm^3) connected with it through a valve. The catalyst sample (0.1–0.3 g) was placed into this reactor. All this together formed the reaction space with the overall volume of 683 cm^3 connected with the bulb containing isotope gases. The isotope preparation used was gaseous oxygen or carbon dioxide containing a given amount of the ^{18}O isotope. The temperature in the reactor was controlled using an electric furnace. The reaction chamber was equipped with a diffusion and forevacuum pump for evacuation and also with a quadrupole mass-spectrometer (SRS QMS200, Stanford Research Systems, USA) for determination of isotopic composition in the on-line mode with the step of 10 s. The samples were pretreated before the experiments in air at 650°C for 2 h and then in vacuum ($p \sim 10^{-6}$–10^{-7} Torr) at 400°C for 90 min. Two types of isotopic exchange (IE) experiments were carried out: isothermal (IIE) and temperature–programmed (TPIE). In an isothermal experiment, the required amount of the tracer reagent (1.4–2.1 Torr) was transferred from the gas bulb into a preevacuated storage volume, after which the reactor was opened. In TPIE experiments, the linear temperature ramp was established with the rate 5°/min from 100 to 750°C.

Isotopic exchange in flow–through reactor. The flow–through device consisted of a tube reactor, tube furnace with a Miniterm thermostat controller, gas line, gas supply block (Flow Mass Controller), a system of taps for the switching of gas flows, UGA-200 quadrupole mass spectrometer (Stanford Research Systems, USA), and two personal computers with installed software for control of the gas supply block (ChemLab3) and a mass-spectrometer (UGA3 and RGA3). A sample in the form of granules with the size of 0.25–0.5 mm was placed into a tube quartz reactor. The sample was pretreated in the flow of 1 vol % O_2 in He for 40 min at 700°C. Similar to the case of closed reactor, experiments were carried out in both isothermal and temperature–programmed modes. In the isothermal experiment, the switching to a mixture of 1% $^{18}O_2$ + He or 1% $C^{18}O_2$ + He was carried out under the conditions of established adsorption–desorption equilibrium in the mixture of 1% $^{16}O_2$ + He and changes in the isotopic mixture composition at the reactor outlet were registered. The temperature linear increase mode at the rate of 5°C/min was established in a temperature–programmed experiment after the switching from the initial mixture to the isotopic one.

MODELING OF ISOTOPIC EXCHANGE IN A GAS–OXIDE SYSTEM

If oxygen is represented by two isotopes, ^{16}O and ^{18}O, isotopic redistribution in the O_2–[O] system (here, [O] designates oxygen of the oxide surface) may be described by two independent external exchange reactions: a) redistribution of isotopic molecules in the gas phase as a result of homoexchange and b) redistribution of isotopes between the phases as a result of heteroexchange. These reactions may occur according to three kinetically independent types of mechanisms (exchange types), as dependent on the number of [O] atoms (0, 1, or 2) participating in exchange with oxygen:

1. Homoexchange without participation of the oxide oxygen atoms (type I, the exchange rate is denoted as R^0)

$$^{16}O_2 + {}^{18}O_2 = 2{}^{16}O{}^{18}O.$$

2. Simple heteroexchange with participation of a single oxide oxygen atom (type II, R^1)

$$^{18}O_2 + [{}^{16}O] = {}^{16}O{}^{18}O + [{}^{18}O].$$

3. Complex (two–stage exchange) with participation of two oxide oxygen atoms (type III, R^2)

$$^{18}O_2 + 2[{}^{16}O] = {}^{16}O_2 + 2[{}^{18}O].$$

The concepts of exchange types introduced by Klier [23] and Muzykantov [24] for description of processes of isotopic exchange between oxides and dioxygen are also applicable to exchange with CO_2. As a rule, isotopic exchange of oxygen on the oxide surface is accompanied by diffusion of tracer atoms into the bulk.

In a general case, the model of isotopic exchange between the oxygen-containing gas–phase reagent (O_2 or CO_2) and oxide oxygen can be presented as follows:

$$\frac{\partial \alpha_g}{\partial t} + O(\tau) = \frac{N_s}{N_g} R^{\Sigma}(\alpha_s - \alpha_g), \quad (1)$$

$$\frac{\partial \alpha_s}{\partial t} = R^{\Sigma}(\alpha_g - \alpha_s) - \frac{N_{bulk}}{N_s}\frac{D}{h^2}\frac{\partial \alpha_{bulk}}{\partial \eta}\bigg|_{\eta = 0}, \quad (2)$$

$$\frac{\partial \alpha_{bulk}}{\partial t} = \frac{D}{h^2}\frac{\partial^2 \alpha_{bulk}}{\partial \eta^2}, \quad (3)$$

$$\frac{\partial f_{16-18}}{\partial t} + O(\tau) = R^0(2\alpha_g(1-\alpha_g) - f_{16-18}) + \frac{N_s}{N_g}(R^2(2\alpha_s(1-\alpha_s) - f_{16-18}) + R^1(\alpha_g(1-\alpha_s) + \alpha_s(1-\alpha_g) - f_{16-18})). \quad (4)$$

The initial conditions are: at $t = 0$ $\alpha_i = \alpha_i^0$.

Here, α_g, α_s, and α_{bulk} are atomic fractions of ^{18}O in the gaseous reagent on the oxide surface and in its bulk, respectively; N_g, N_s, and N_{bulk} is the amount of oxygen atoms in the gas phase, on the oxide surface and in its bulk; f_{16-18} is the molecular fraction of $^{16}O^{18}O$ (in case of exchange with O_2) or $C^{16}O^{18}O$ (in case of carbon dioxide); R^0, R^1, R^2 are the rates of various exchange types; $R^{\Sigma} = 0.5R^1 + R^2$ is the overall heteroexchange rate, D is the diffusion coefficient, h is the characteristic oxide particle size, η is the dimensionless value of distance from the surface; t is the time; $O(\tau)$ is an operator depending on the mass transport mode in a reactor:

$$O(\tau) = \begin{cases} 0 & \text{in a static reactor} \\ \dfrac{1}{\tau}\dfrac{\partial \alpha_g (\text{or } f_{16-18})}{\partial \xi} & \text{in a flow-through} \\ & \text{displacement reactor.} \end{cases}$$

Here, τ is the contact time in the reactor, ξ is the dimensionless catalyst layer length.

In the isothermal case, the exchange rates and diffusion coefficients are assumed to be constant. Exchange rates and diffusion coefficients are expressed using an Arrhenius dependence to describe temperature–programmed experiments:

$$R^{(i)} = R^{(i)}_{ref} e^{-\frac{E_{R(i)}}{RT}}, \quad D = D_{ref} e^{-\frac{E_D}{RT}}, \quad T' = \frac{TT_{ref}}{T_{ref} - T},$$

where $R^{(i)}_{ref}$ and D_{ref} are exchange rates and the diffusion coefficient at temperature T_{ref}; $E_{R(i)}$ and E_D are activation energies.

The suggested model (1)–(4) allows performing within a unified approach numeric analysis of isotope experiments implemented in reactors of different types in different temperature modes and using different oxygen–containing reagents.

Let us point out that at $N_{bulk}D/h^2 \gg N_sR^{\Sigma}$, equations (1)–(3) are reduced to the following form:

$$\frac{\partial \alpha_g}{\partial t} + O(\tau) = \frac{N_{bulk} + N_s}{N_g} R^{\Sigma}(\alpha_s - \alpha_g), \quad (5)$$

$$\frac{\partial \alpha_s}{\partial t} = R^{\Sigma}(\alpha_g - \alpha_s) \quad (6)$$

and thus, we can pass to the so called "uniform" isotopic exchange model assuming that all atoms of the solid that are capable of being exchanged are equivalent. Therefore, within our approach, the "uniform" model is a special case of the general diffusion model (1)–(4), when diffusion of the isotopic label into the bulk occurs so fast (as compared to exchange on the surface) that the degree of isotopic oxygen exchange on the oxide surface and in its whole bulk is the same. At $O(\tau) = 0$, equations (5), (6) can be solved analyti-

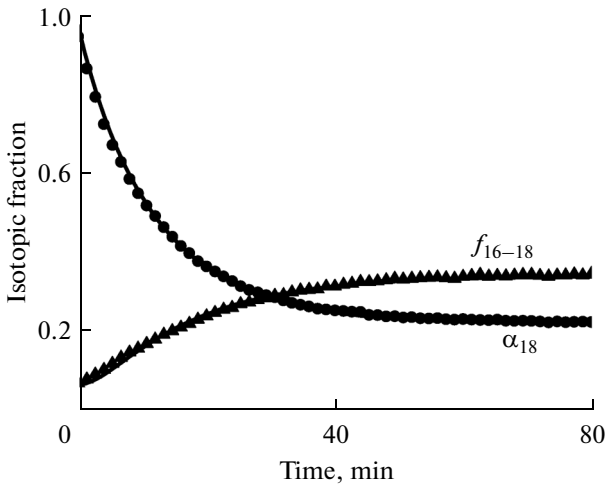

Fig. 1. Isotopic exchange with $^{18}O_2$ in a closed reactor at 700°C on $Pt/Pr_{0.3}Ce_{0.35}Zr_{0.35}O_2$. Variation of the atomic fraction of ^{18}O (α_{18}) and molecular fraction of $^{16}O^{18}O$ (f_{16-18}) as dependent on time. Here and further: the points correspond to the experiment and the lines correspond to calculations.

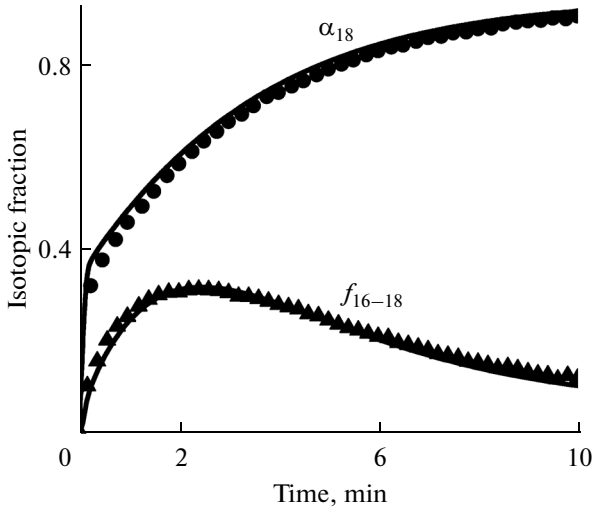

Fig. 2. Isotopic exchange with $^{18}O_2$ in a flow–through reactor at 700°C on $Pt/Pr_{0.3}Ce_{0.35}Zr_{0.35}O_2$. Variation of the atomic fraction of ^{18}O (α_{18}) and molecular fraction of $^{16}O^{18}O$ (f_{16-18}) as dependent on time.

cally and we obtain the classical equation of homogeneous isotopic oxygen exchange in a closed reactor:

$$\alpha_g = \gamma + (\alpha_g^0 - \gamma)\exp(-1(1+\lambda)Rt),$$

here, γ is the equilibrium faction of the isotope and $\lambda = N_g/N_{oxide}$.

RESULTS AND DISCUSSION

Doped Cerium–Zirconium Mixed Oxides with a Fluorite–Type Structure (at the Example of $Pt/Pr_{0.3}Ce_{0.35}Zr_{0.35}O_2$)

The $Pt/Pr_{0.3}Ce_{0.35}Zr_{0.35}O_2$ sample was tested in the reaction of isotopic exchange with $^{18}O_2$ and $C^{18}O_2$. Experiments were carried out in a static and flow–through device in isothermal and temperature–programmed modes. In case of exchange with $^{18}O_2$ in a closed reactor in the isothermal mode (t = 700°C), atomic fraction $\alpha_{18}(t)$ of ^{18}O in the gaseous oxygen decreased exponentially and was described by a uniform isotopic exchange model (Fig. 1). This means that the rate of self-diffusion of oxygen atoms in the sample bulk is much higher than the rate of oxygen exchange on the surface. However, as the substitution degree of oxide oxygen in this experiment did not exceed 20%, one could not exclude the presence of a certain amount of relatively slowly substituted oxide oxygen.

With account for ambiguity of the results obtained in a closed reactor, the further studies were carried out in a flow–through setup, which allowed bringing the oxygen substitution degree in the oxide closer to 100%. Figure 2 shows the results with the experiment with $^{18}O_2$ in a flow–through reactor at t = 700°C. In a certain time period after the switching of flows from $^{16}O_2$ + He to $^{18}O_2$ + He corresponding to the reactor purging time, oxygen isotopes are registered at the reactor outlet. However, the fraction of ^{18}O in gaseous oxygen at the reactor outlet is much lower than at the inlet, which points to intense isotopic exchange with the oxide oxygen. The difference between the isotopic fraction and the reactor inlet and outlet is determined by heteroexchange rate R^{Σ} (in the isothermic experiment, R^{Σ} = const) and degree of deviation from isotopic equilibrium between the gas phase and surface ($\alpha_g - \alpha_s$). As oxide oxygen is substituted, difference ($\alpha_g - \alpha_s$) decreases, the system gradually approaches isotopic equilibrium and isotopic fraction of ^{18}O in O_2 at the outlet approaches its value in the inlet flow. Similar experiments were carried out at 500 and 600°C. Numeric analysis shows that the dynamics of response $\alpha_{18}(t)$ and $f_{16-18}(t)$ in all experiments are described by a uniform model according to the third–type mechanism which includes the stage of molecular oxygen predissociation. Hence, isotopic exchange of oxygen in a sample in case of exchange with $^{18}O_2$ in the studied temperature sample is largely limited by a comparatively low rate of O_2 dissociation. Consequently, oxygen self-diffusion coefficients in this case cannot be determined.

As opposed to $^{18}O_2$, the dynamics of response $\alpha_g(t)$ in case of exchange with $C^{18}O_2$ (Fig. 3) cannot be described by a uniform model (dashed line). A satisfactory description could be obtained only within a complete model accounting for diffusion limitations for oxygen substitution within the bulk of the sample (solid line). Besides, as shown by analysis of the

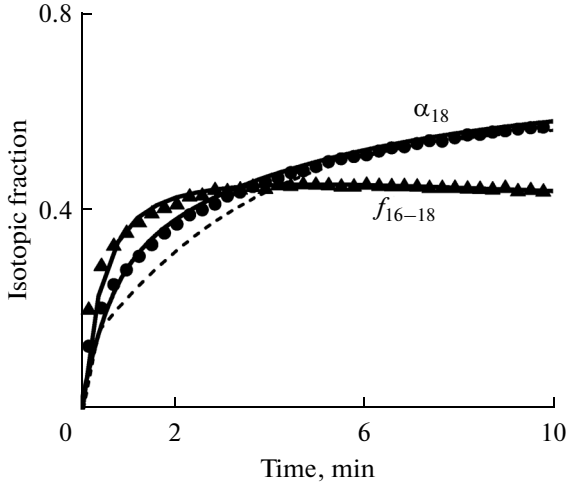

Fig. 3. Isotopic exchange with $C^{18}O_2$ in a flow–through reactor at 700°C on $Pt/Pr_{0.3}Ce_{0.35}Zr_{0.35}O_2$. Variation of the atomic fraction of ^{18}O (α_{18}) and molecular fraction of $C^{16}O^{18}O$ (f_{16-18}) as dependent on time.

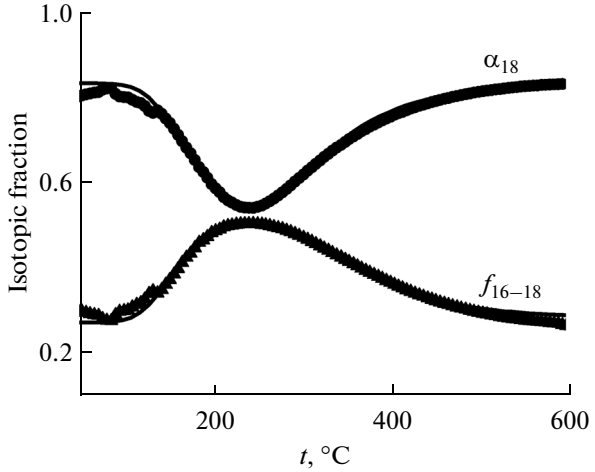

Fig. 4. Temperature–programmed isotopic exchange with $C^{18}O_2$ in a flow–through reactor $Pt/Pr_{0.3}Ce_{0.35}Zr_{0.35}O_2$. Variation of the atomic fraction of ^{18}O (α_{18}) and molecular fraction of $C^{16}O^{18}O$ (f_{16-18}) as dependent on temperature.

dependence of $f_{16-18}(t)$, exchange between $C^{18}O_2$ and surface oxygen occurs via the second–type mechanism without predissociation of the CO_2 molecule.

As follows from our estimates, when isotopic reagent $C^{18}O_2$ is used, the rate of isotopic exchange on the surface of the given sample increases by at least an order of magnitude, while actually allows estimating the rate of the diffusion process.

The most complete pattern of oxygen exchange dynamics is provided by the data of temperature–programmed exchange with $C^{18}O_2$ in a flow–through reactor (Fig. 4). Up to the temperature of approximately 100°C, isotopic composition of CO_2 in case of its passing through a sample layer remains unchanged and corresponds to the isotopic composition of the mixture at the reactor inlet, i.e., the rate of oxygen exchange is too low to cause significant changes in the gas–phase isotopic composition. At an increase in the temperature, the exchange rate grows and, starting from 100°C, we observe a decrease in the fraction of ^{18}O in CO_2 (α_{18}) at the reactor outlet. Then, as oxide oxygen is substituted, the system gradually passes to isotopic equilibrium and response curves $\alpha_g(t)$ and $f_{16-18}(t)$ contain extremums, after which the level corresponding to the isotopic composition of the inlet mixture is reached.

Numerical analysis of temperature–programmed experiments with $C^{18}O_2$ showed that oxide oxygen substitution is limited by the surface exchange in the initial time period at relatively low temperatures. Due to high (about 100 kJ/mol) activation energy, the surface exchange rate grows drastically at an increase in the temperature and oxygen bulk diffusion becomes the limiting stage at $t > 300$°C with its activation energy being much lower, about 40 kJ/mol.

If diffusion path length h is assumed to be the radius of catalyst particles ($r = 3V/S = 6 \times 10^{-6}$ cm, where V is the volume, S is the surface area), the calculated diffusion coefficient D at 500°C is $\approx 2 \times 10^{-12}$ cm^2/s. The obtained value exceeds by several orders of magnitude the estimates of diffusion coefficients on oxides with close chemical composition available in the literature [25]. Such a high mobility is due to large area of interdomain boundaries, along which fast transport of oxygen atoms from the particle surface to the surface of individual domains occurs [6].

Doped Lanthanum Silicates with an Apatite–Type Structure

Same as in fluorites, exchange of apatites with $^{18}O_2$ in the whole studied temperature region (200–700°C) was limited by the stage of molecular oxygen adsorption. When $C^{18}O_2$ was used as an isotopic reagent, the exchange rate increased significantly. In the range of temperatures up to 300–400°C (as dependent on the sample), the exchange rate of apatite oxygen was controlled by surface reaction, while bulk diffusion limits this rate at higher temperature. It was assumed on the basis of the catalyst structure that a part of apatite oxygen, namely interstitial oxygen, must be replaced faster than oxygen in the regular sites [15, 16]. However, numeric analysis revealed no significant differences in the rate of substitution of different lattice oxygen types. The response dynamics was described by a diffusion model with a single oxygen form in the particle bulk. As an example, the data of temperature–programmed exchange with $C^{18}O_2$ in a flow–through reactor for $La_{10}Si_{5.5}Fe_{0.5}O_{26}$ sample annealed at 1200°C are presented (Fig. 5). Equivalence of all oxygen atoms

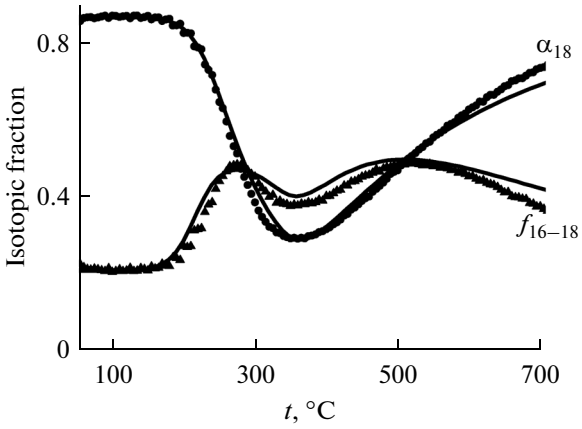

Fig. 5. Temperature–programmed isotopic exchange with $C^{18}O_2$ in a flow–through reactor $La_{10}Si_{5.5}Fe_{0.5}O_{26}$. Variation of the atomic fraction of ^{18}O (α_{18}) and molecular fraction of $C^{16}O^{18}O$ (f_{16-18}) as dependent on temperature.

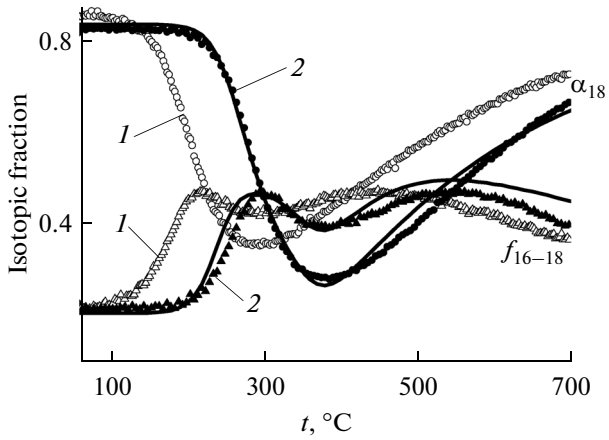

Fig. 6. Temperature–programmed isotopic exchange with $C^{18}O_2$ in a flow–through reactor on the $La_{9.83}Si_5Al_{0.75}Fe_{0.25}O_{26.5}$ sample sintered at (*1*) 900°C and (*2*) 1200°C. Variation of the atomic fraction of ^{18}O (α_{18}) and molecular fraction of $C^{16}O^{18}O$ (f_{16-18}) as dependent on temperature.

in the apatite bulk with respect to isotopic exchange supports the model, in which oxygen mobility is determined by nonlinear cooperative process of oxygen ion migration between interstitial and tetrahedral sites. Herewith, the calculated oxygen self-diffusion coefficient in apatites is approximately two orders of magnitude higher as compared to doped cerium–zirconium oxides with a fluorite structure, which is confirmed by the SIMS data [26]. Let us point out that partial substitution of Fe by Al causes a certain decrease in the oxygen self-diffusion rate in apatites (see Table 1).

The effect of sample annealing temperature on the kinetics of isotopic exchange with $C^{18}O_2$ was also studied. As seen in Fig. 6, isotopic exchange shifts towards higher temperatures at an increase in the sample annealing temperature, i.e., the observed exchange rate decreases. Numeric analysis of isotopic exchange showed that the observed decrease in the exchange rate is related solely to a decrease in the surface exchange rate due to sintering, while the rate of oxygen self diffusion in this case even increases.

Earlier, such a trend, i.e., an increase in specific conductivity, and thus an increase of the oxygen self-diffusion coefficient at an increase in the annealing temperature of aluminum– and iron–codoped lanthanum silicate samples with an apatite structure was pointed out in [15].

For aluminum– and iron–doped samples of lanthanum silicates with an apatite structure annealed at 1450°C, estimation of oxygen self-diffusion coefficient on the basis of the specific conductivity data in [15] (~10^{-4} S/cm at 500°C) yields the values of $D_O \sim (2–3) \times 10^{-10}$ cm^2/s, which also agrees with the estimates according to the method of temperature–programmed isotopic exchange with $C^{18}O_2$ in a flow–through reactor.

Mixed Praseodymium Nickelates–Cobaltites and Their Composites

According to the XRD data, samples of $PrNi_{1-x}Co_xO_{3+\delta}$ have a perovskite structure, ABO_3, with a small amount (up to 10%) of impurity phases: Pr_6O_{11}, NiO, and phases with a Ruddlesden–Popper structure (homolog of $A_4B_3O_{10}$) [20].

As opposed to fluorites and apatites discussed above, perovskites activate oxygen comparatively easily and diffusion processes affect substantially dynamics of exchange with $^{18}O_2$ in the high–temperature region. As to exchange with $C^{18}O_2$, in this case, substitution of oxygen in perovskite in the whole studied temperature range of 100–800°C is fully controlled by diffusion. This is a rare case when the effect of diffusion is manifested even in a static experiment. Thus, e.g., the dependence of $\alpha_g(t)$ in a temperature-programmed experiment in a closed reactor (Fig. 7) contains 2 regions corresponding to two forms of perovskite oxygen with considerably differing rates of isotopic substitution. According to approximate estimates, a relatively small fraction of oxygen (less than 20%) is substituted by at least an order of magnitude faster than that of the major part of perovskite oxygen.

The presence of two oxygen forms is most visibly manifested in temperature–programmed experiments in a flow–through reactor (Fig. 8). The dependence of $\alpha_g(t)$ contains two pronounced peaks of ^{18}O absorption from the gas phase: a relative small low-temperature peak and the main high-temperature peak. Numeric analysis was used to determine diffusion coefficients

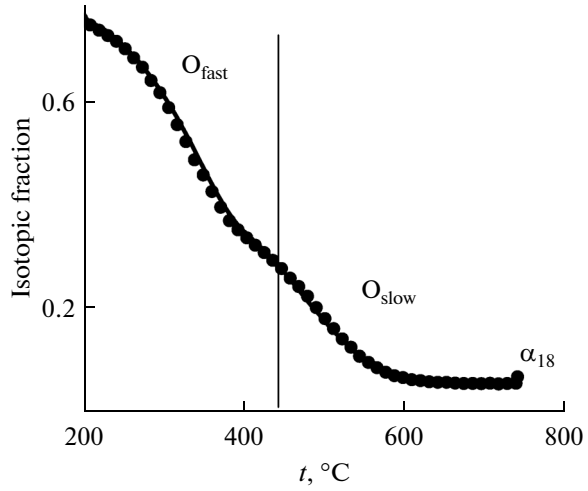

Fig. 7. Temperature–programmed isotopic exchange with $C^{18}O_2$ in a closed reactor on a $PrNi_{0.5}Co_{0.5}O_{3+\delta}$ sample. Variation of the atomic fraction of ^{18}O (α_{18}) and molecular fraction of $C^{16}O^{18}O$ (f_{16-18}) as dependent on temperature.

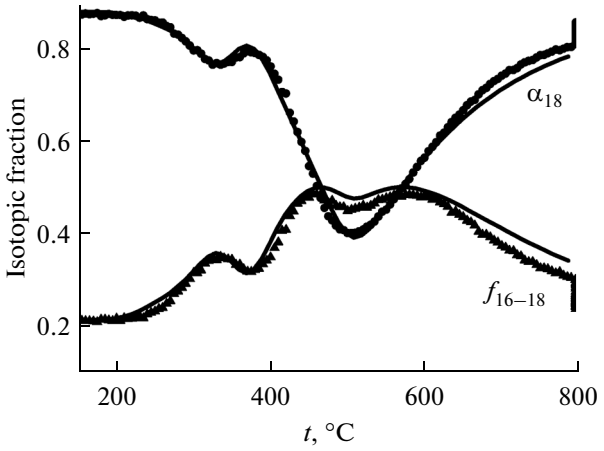

Fig. 8. Temperature–programmed isotopic exchange with $C^{18}O_2$ in a flow–through reactor on $PrNi_{0.5}Co_{0.5}$. Variation of the atomic fraction of ^{18}O (α_{18}) and molecular fraction of $C^{16}O^{18}O$ (f_{16-18}) as dependent on temperature.

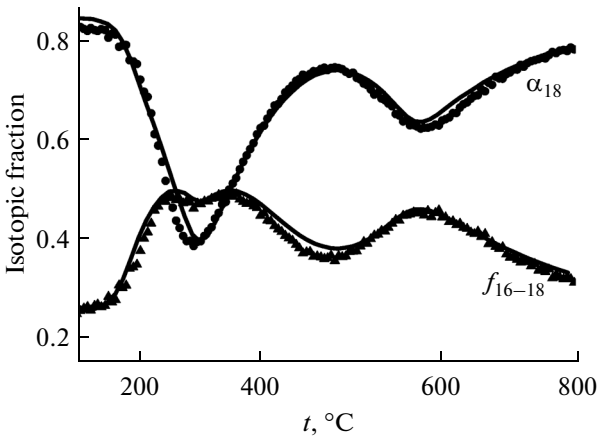

Fig. 9. Temperature–programmed isotopic exchange with $C^{18}O_2$ in a flow–through reactor on a $PrNi_{0.5}Co_{0.5}$–YDC composite sample. Variation of the atomic fraction of ^{18}O (α_{18}) and molecular fraction of $C^{16}O^{18}O$ (f_{16-18}) as dependent on temperature.

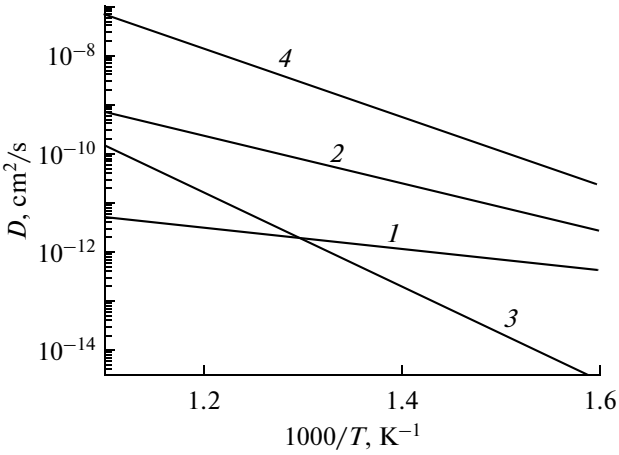

Fig. 10. Arrhenius dependences of oxygen self-diffusion coefficients in various oxide systems: (*1*) $Pt/Pr_{0.3}Ce_{0.35}Zr_{0.35}O_2$ with a fluorite-type structure, (*2*) $La_{10}Si_{5.5}Fe_{0.5}O_{26.5}$ with an apatite-type structure, (*3*) oxygen in a $PrNi_{0.5}Co_{0.5}$ sample corresponding to the perovskite structure (without account for the impurity phase), (*4*) the bulk (60%) of oxygen in the composite of $PrNi_{0.5}Co_{0.5}O_3 + CeYO_2$.

characterizing different oxygen forms and their percentage in different $PrNi_{1-x}Co_xO_{3+\delta}$ samples (Table 2).

As seen in Table 2, the amount of fast exchanging oxygen in all samples is approximately 5–10% and can probably be assigned to the impurity phase with a Ruddlesden–Popper structure and/or defects in the perovskite structure.

The amount of fast substituted oxygen clearly increases as compared to PrNiCo in perovskite–fluorite composites (Fig. 9). The calculated values of diffusion coefficients characterizing different forms of oxygen in composite samples are presented in Table 2. As seen from the data of Table 2, the diffusion coefficient characterizing the most mobile oxygen fraction in the composite corresponding to about 60% of the stoichiometric oxygen amount in the sample also increases. Herewith, this diffusion coefficient greatly exceeds those of all systems with fluorite, apatite, and perovskite structure studied in this work (Fig. 10).

We believe that an increase in the oxygen diffusion rate in the composite is related to:

• well-developed interface serving as a fast oxygen diffusion channel,

• incorporation of praseodymium cations into the fluorite structure and distortion of the perovskite structure, which results in the weakening of the bond between oxygen in the anion sublattice and the surrounding metal cations.

It is important to point out that nanocomposites based on mixed praseodymium nickelates–cobaltites with doped cerium oxide demonstrate very high mobility and reactivity of oxygen exceeding the corresponding characteristics for conventional complex perovskites doped by strontium (LSCF etc.). The key role in development of fast diffusion channels in systems based on praseodymium nickelates–cobaltites is played by the structure disordering processes, including those due to redistribution of cations between perovskite and fluorite domains and also processes of segregation of nickel cations from the perovskite structure under high–temperature sintering [20].

CONCLUSIONS

It is shown at the example of dispersed oxide systems with different composition and structure type, i.e., doped cerium–zirconium oxides with a fluorite-type structure, doped lanthanum silicates with an apatite-type structure, and also mixed praseodymium nickelates–cobaltites and their nanocomposites with yttrium–doped ceria, that temperature–programmed exchange with $C^{18}O_2$ in a flow–through reactors is the most efficient methods of studying oxygen mobility in oxides. It allows determining not only the average integral value of oxygen self-diffusion coefficients, but also detecting oxygen forms with different mobility in the solid bulk, which is especially important for composite materials. This is related to high rate of the surface reaction of CO_2 exchange with surface oxygen via the second-type mechanism not requiring dissociation of the CO_2 molecule, which may be related to formation of carbonate complexes. As a result, the overall rate of oxide oxygen heteroexchange with $C^{18}O_2$ in the gas phase is controlled by bulk diffusion of oxide particles, while heteroexchange with $^{18}O_2$ is mainly limited by the surface reaction with the bond rupture in the oxygen molecule, which hinders calculation of bulk diffusion parameters. For doped lanthanum silicates with an apatite structure, good agreement between the obtained values of self-diffusion coefficients and the data obtained for compact samples with close composition by methods of SIMS and conductivity measurements was demonstrated. For these electrolytes with different structural types of lattice oxygen, exchange is well described by a single diffusion coefficient, which agrees with the cooperative diffusion mechanism with participation of oxygen atoms both in the regular and interstitial positions.

ACKNOWLEDGMENTS

The authors are grateful to the Ministry of Education and Science of the Russian Federation for financial support of this work.

REFERENCES

1. Muzykantov, V.S., Popovskii, V.V., and Boreskov, G.K., *Kinet. Catal,* 1964, vol. 5, p. 624.
2. Ozaki, A., *Isotopic Studies of Heterogeneous Catalysis*, New York: Academic Press, 1977.
3. Sadovskaya, E.M., Bulushev, D.A., and Bal'zhinimaev, B.S., *Kinet. Catal.*, 1999, vol. 40, p. 54.
4. Klier, K. and Kucera, E., *J. Phys. Chem. Solids*, 1966, vol. 27, p. 1087.
5. Galdicas, A., Descorme, C., and Duprez, D., *Solid State Ionics*, 2004, vol. 166, p. 147.
6. Sadovskaya, E.M., Ivanova, Y.A., Pinaeva, L.G., Kuznetsova, T.G., Sadykov, V.A., Grasso, G., Van Veen, A., and Mirodatos, C., *J. Phys. Chem. A,* 2007, vol. 111, p. 4498.
7. Sadovskaya, E.M., Goncharov, V.B., Gulyaeva, Yu.K., Popova, G.Ya., and Andrushkevich, T.V., *J. Mol. Catal. A: Chem.*, 2010, vol. 316, p. 118.
8. Frolov, D.D., Kotovshchikov, Y.N., Morozov, I.V., Boltalin, A.I., Fedorova, A.A., Marikutsa, A.V., Rumyantseva, M.N., Gaskov, A.M., Sadovskaya, E.M., and Abakumov, A.M., *J. Solid State Chem.*, 2012, vol. 186, p. 1.
9. Ivanov, D.V., Pinaeva, L.G., Sadovskaya, E.M., and Isupova, L.A., *Kinet. Catal.*, 2001, vol. 52, p. 401.
10. Sadykov, V.A., Sazonova, N.N., Bobin, A.S., Muzykantov, V.S., Gubanova, E.L., Alikina, G.M., Lukashevich, A.I., Rogov, V.A., Sadovskaya, E.M., Mezentseva, N.V., Veniaminov, S.A., Ermakova, E.N., Zevak, E.G., Muhler, M., Van Veen, A.C., Mirodatos, C., and Schuurman, Y., *Catal. Today*, 2011, vol. 169, p. 125.
11. Sadykov, V., Muzykantov, V., Bobin, A., Mezentseva, N., Alikina, G., Sazonova, N., Sadovskaya, E., Gubanova, L., Lukashevich, A., and Mirodatos, C., *Catal. Today*, 2010, vol. 157, p. 55.
12. Nakayama, S. and Sakamoto, M., *J. Eur. Ceram. Soc.,* 1998, vol. 18, p. 1413.
13. Leon-Reina, L., Porras-Vazquez, J.M., Losilla, E.R., and Aranda, M.A.G., *Solid State Ionics*, 2006, vol. 177, p. 1307.
14. Kendrick, E., Islam, M.S., and Slater, P.R., *J. Mater. Chem.,* 2007, vol. 17, p. 3104.
15. Sadykov, V., Kharlamova, T., Mezentseva, N., Pavlova, S., Sadovskaya, E., Muzykantov, V., Bespalko, Yu., Usol'tsev, V., Zevak, E., Kriger, T., Ishchenko, A., Uvarov, N., Ulikhin, A., Chaikina, M., and Argirusis, C., *Russ. J. Electrochem.*, 2011, vol. 47, p. 427.
16. Kharlamova, T., Pavlova, S., Sadykov, V., Chaikina, M., Krieger, T., Ishchenko, A., Pavlukhin, Y., Petrov, S., and Argirusis, C., *Eur. J. Inorg. Chem.*, 2010, p. 589.
17. Huang, Sh., Lu, Q., Feng, Sh., Li, G., and Wang, Ch., *J. Power Sources*, 2012, vol. 199, p. 150.

18. Hjalmarsson, P. and Mogensen, M., *J. Power Sources,* 2011, vol. 196, p. 7237.

19. Ferchaud, C., Grenier, J.-C., Zhang-Steenwinkel, Y., van Tuel, M.M.A., van Berkel, F.P.F., and Bassat, J.-M., *J. Power Sources*, 2011, vol. 196, p. 1872.

20. Sadykov, V.A., Eremeev, N.F., Sadovskaya, E.M., Bobin, A.S., Fedorova, Yu.E., Muzykantov, V.S., Mezentseva, N.V., Alikina, G.M., Kriger, T.A., Belyaev, V.D., Rogov, V.A., Ulikhin, A.S., Okhlupin, Yu.S., Uvarov, N.F., Bobrenok, O.F., McDonald, N., Watton, J., Dhir, A., Steinberger-Wilckens, R., Mertens, J., and Vinke, I.C., *Russ. J. Electrochem.*, 2014, vol. 50, p. 669.

21. Kuznetsova, T.G., Sadykov, V.A., Veniaminov, S.A., Alikina, G.M., Moroz, E.M., Rogov, V.A., Martyanov, O.N., Yudanov, V.F., Abornev, I.S., and Neophytides, S., *Catal. Today*, 2004, vol. 161, p. 91.

22. Sadykov, V., Kuznetsova, T.G., Muzykantov, V.S., Pinaeva, L.G., Paukshtis, E.A., Mezentseva, N.V., Kemnitz, E., Mirodatos, C., and van Veen, A.C., *Catal. Today*, 2006, vol. 117, p. 475.

23. Klier, K., Novakova, J., and Jiru, P., *J. Catal.*, 1963, vol. 2, p. 479.

24. Muzykantov, V.S., Jiru, P., Klier, K., and Novakova, J., *Collect. Czech. Chem. Commun.*, 1968, vol. 33, p. 829.

25. Dong, F., Suda, A., Tanabe, T., Nagai, Y., Sobukawa, H., Shinjoh, H., Sugiura, M., Descorme, C., and Duprez, D., *Catal. Today*, 2004, vol. 827, p. 93.

26. Argirusis, C., Jothinathan, J., Sourkouni, E., Van der Biest, O., and Jomard, F., *Solid State Ionics*, 2014, vol. 257, p. 53.

Translated by M. Ehrenburg